

Multiphysical modelling of keyhole formation during dissimilar laser welding

I. Tomashchuk^{1*}, I. Bendaoud¹, P. Sallamand¹, E. Cicala¹, S. Lafaye², M. Almuneau²

¹Laboratoire Interdisciplinaire Carnot de Bourgogne (ICB), UMR 6303 CNRS - Université de Bourgogne – Franche Comté, 12, rue de la Fonderie – 71200 Le Creusot, France

²Laser Rhône-Alpes-5, rue du Rif Tronchard - 38120 Le Fontanil, France

* iryana.tomashchuk@u-bourgogne.fr

Abstract: In the present study, time-dependent multiphysical simulation of pulsed and continuous laser welding of dissimilar metals, based on Moving Mesh approach, is proposed. Strong coupling between heat transfer, laminar compressible flow and ALE is used. The model allows following the thermal field, free surface deformation and convection phenomena during the development of melted zone.

In the first place, the model was applied to a case of single material (Ti6Al4V alloy) and successfully validated by comparison with experimental weld dimensions. Next, the model was applied for studying of keyhole dynamics and melted zone development in a case of dissimilar materials, in pulsed and continuous laser mode. The effect of discontinuity of physical properties across the joint line on keyhole behavior was studied for dissimilar couple Ti6Al4V/stainless steel.

Keywords: laser, metallic alloys, dissimilar welding, multiphysics.

1. Introduction

The development of melted zone during high power laser welding of metallic materials is strongly affected by shape and dimensions of vapor-filled keyhole that forms during laser-matter interaction¹. In case of bimetallic joining of metals and alloys, the discontinuity of physical properties (like laser absorption coefficient, thermal diffusivity, phase change temperatures etc.) may lead to the dissymmetry of the keyhole relatively to joint line. Very few experimental and numerical studies deal with this phenomenon, which is quite important for control of elemental composition and, consequently, of tensile properties of dissimilar welds.

Multiphysical modelling can be an important tool for comprehension of welding mechanisms²

and improving weld quality³. Few studies dedicated to numerical modelling of high power beam welding of dissimilar materials, are based on fixed keyhole approach⁴ (means, a keyhole is introduced as a fixed geometry) or on equivalent source approach with no cavity⁵. Recently, free surface models using ALE and phase field approach were proposed by Bruyere et al⁶. Coupled resolution of heat transfer, fluid flow and mesh deformation problems allowed following the evolution of pulsed weld and predict possible defect formation.

The present numerical study aims to reproduce the development of melted zone between dissimilar materials during pulsed and continuous welding mode. For validation of the model, an experimental study was carried out.

2. Governing equations

2.1 Heat transfer

Heat transfer equation was used in time-dependent form:

$$\rho c_p \text{eq} \left(\frac{\partial T}{\partial t} + \vec{u} \cdot \vec{\nabla} T \right) = \vec{\nabla} \cdot (\lambda \vec{\nabla} T) \quad (1)$$

Laser energy supply is represented by Gauss heat source applied at the top of butt joint. Pulsed laser beam is represented as follows:

$$q_L = \frac{P_L A}{\pi r_0^2} e^{-\left(\frac{x^2+y^2}{r_0^2}\right)} \cdot (t < t_{pulse}), \quad (2)$$

where P_L – laser power, r_0 – beam radius and t_{pulse} – pulse duration A - absorption coefficient of laser radiation by each individual material, represented as :

$$A = A_{solid} + (A_{liquid} - A_{solid}) \cdot f_{lc} 2hs(T - T_m, \Delta T), \quad (3)$$

where absorption in liquid phase takes in account the trapping of photons in the keyhole starting from defined critical penetration z_c :

$$A_{liquid} = A_{surf} + (A_{kh} - A_{surf}) \cdot f_{lc} 2hs(z - z_c, \Delta z). \quad (4)$$

For continuous laser welding, moving heat source is given like:

$$q_L = \frac{P_L A}{\pi r_0^2} e^{\left(-\frac{(x+V_w \cdot t)^2 + y^2}{r_0^2}\right)}, \quad (5)$$

where V_w is the velocity of welding.

Latent heat of fusion and evaporation are taken in account by means of equivalent enthalpy approach⁷:

$$c_p^{eq} = c_p + D_m \cdot L_m + D_v \cdot L_v \quad (6)$$

where C_p is heat capacity as function of temperature, L_f and L_v – latent heat of fusion and evaporation and D_f and D_v are Gauss functions normalized around melting and evaporation temperatures T_m and T_v respectively:

$$D_i = \frac{e^{-\frac{(T-T_i)^2}{\Delta T}}}{\sqrt{\pi \Delta T^2}} \quad (7)$$

where ΔT is smoothing interval of 50 K.

Materials properties of Ti6Al4V and 316 L stainless steel are considered as interpolation functions of temperature⁸. In present stage of model development, mixing process is not taken into account.

2.2 Fluid flow

Liquid metal is assumed as incompressible Newtonian liquid that undergoes laminar flow:

$$\rho_l \left[\frac{\partial \vec{u}}{\partial t} + (\vec{u} \cdot \nabla) \vec{u} \right] = \nabla \cdot \left[-pI + \mu(T) (\nabla \vec{u} + (\nabla \vec{u})^T) \right] + \vec{F} \quad (8)$$

$$\nabla \cdot \vec{u} = 0$$

Metal that has $T < T_m$ is considered as highly viscous fluid ($\mu_s = 100$ Pa.s), that practically stops all convection movements in solid materials. The transition between solid and liquid material is provided with smoothed Heaviside function:

$$\eta = \eta_{solid} + (\eta_{liquid} - \eta_{solid}) \text{flc2hs}(T - T_m, \Delta T). \quad (9)$$

Convection movements are generated by following phenomena:

- natural convection described through Boussinesq approximation,
- surface tension force,
- Marangoni convection with $\frac{\partial \gamma}{\partial T} < 0$ introduced in form of weak formulation,
- recoil pressure of vapor filling the keyhole, represented in form of functions of type

$$p_r = a \cdot e^{-\frac{b}{T} + c} \quad (10)$$

proposed by Kaidalov⁹ for a number of metals.

2.3 Free surface

Present study uses ALE moving mesh approach for representing the movements of free surface. The advantage of this method consists in possibility to neglect the vapor phase and thus lighten the calculation. The weak point consists in limitations of free surface movement: the formation of droplets or bubbles in the melted zone is forbidden by the impossibility to break or unite individual meshes. Movement of free surface is above all determined by surface tension and recoil pressure.

3. Use of COMSOL Multiphysics® Software

Present model involves *Heat Transfer in Fluids*, *Laminar flow* and *Moving Mesh* modules that are strongly coupled and solved with time-dependent solver. Multiphysics coupling is ensured by the interrelation between heat transfer and Navier-Stokes equations: velocity field in heat equation is provided by resolution of Navier-Stokes equation, when temperature field defines thermophysical properties of the liquid involved in convection process. Moving Mesh solves surface deformation in function of locally calculated pressure and velocity field.

Welded materials are represented by two 3mm x 2mm x 2mm butt joined domains. Tetrahedral mesh of 300 μm maximal size is applied over calculation domain. The top surface of is meshed with 25 μm. Automatic remesh is applied.

The model is solved on work station with Intel 2.90 (2 processors, 32 cores) and 128 Gb RAM. The longest calculation needed 48 h.

4. Experimental study

Welding experiments were carried out with pulsed Nd:YAG laser of 3 kW maximal power and focused beam diameter \varnothing of 560 μm.

Laser beam was focused on the surface of butt joint between 2 mm thick Ti6Al4V with another Ti6Al4V plate or with 316 L stainless

steel. Standalone pulses with duration of 1-12 ms were realized.

Melted zone development was observed online with high speed camera Phantom (10 000 fps). The penetration of pulses at joint line was measured by breaking the weld and observing Ti6Al4V side of joint plane with optical microscope.

5. Results and discussion

5.1. Validation of the model on homogenous case

In the first place, the model was tested on case of 2 mm thick Ti6Al4V alloy plate that underwent laser pulse of 1.5 kW and 12 ms in duration. Numerically, the development of melted zone with keyhole-like capillary and surrounding ring of ejected liquid has been observed (Figure 1.a).

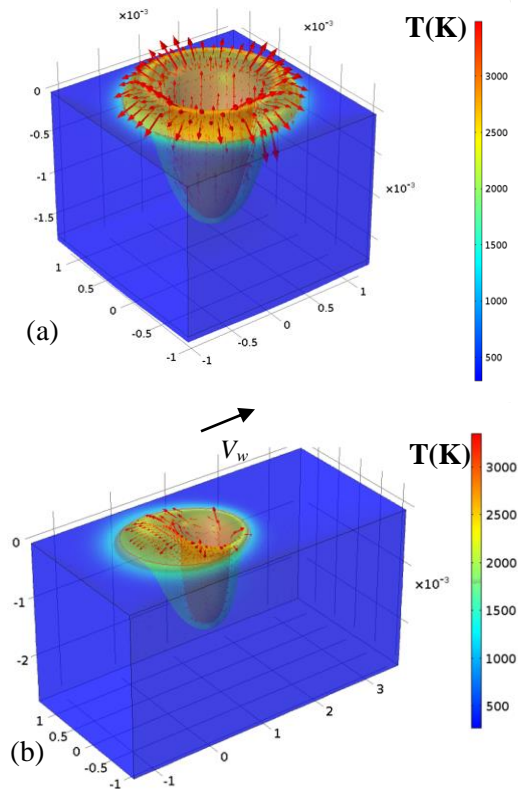


Figure 1. Thermal field of Ti6Al4V plate after 6 ms impact with laser power of 1.5 kW (a) and continuous laser welding with speed of 4 m/min and laser power of 1.5 kW (b).

Maximal calculated temperature attained by the melted zone was 3332 K, which is close to vaporization temperature of Ti6Al4V alloy. Maximal velocity field was observed on keyhole walls and is equal to of 0.7 m/s. Marangoni effect on the borders of the melted zone (average velocity of 0.5 m/s) is superposed with ejection flow during the creation of the keyhole. For validation of the model, impact width and penetration were measured. Figure 2 illustrates satisfactory correspondence in melted zone dimensions between experiment and calculation.

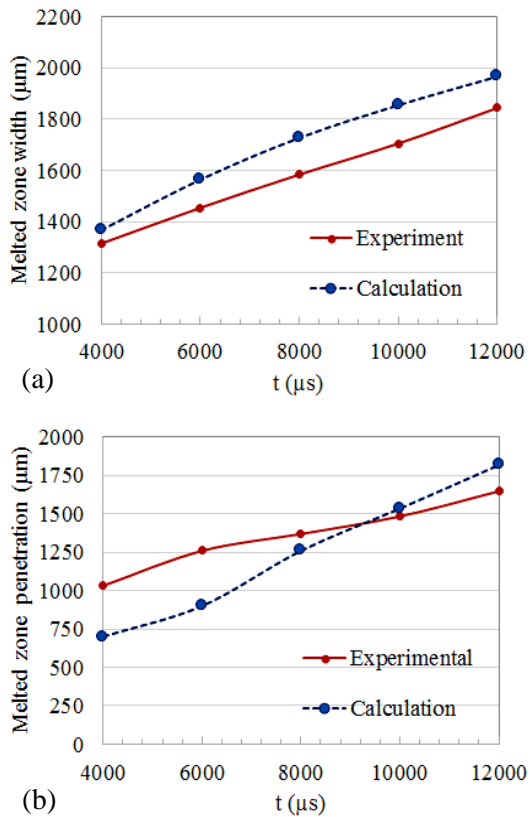


Figure 2. Comparison between experimental and calculated melted zone dimensions for 1.5 kW laser pulse at Ti6Al4V.

Preliminary tests for continuous welding mode (Figure 1.b) also gave promising results: it was possible to follow the advancement of the initiating keyhole in welding direction along with evolution of melted zone. The ejection of melted material past the keyhole and formation of dominant convection vortex was observed.

5.2. Simulation of dissimilar pulsed welding between Ti6Al4V and stainless steel

In case of dissimilar welding, thermal field is uneven on different sides of the joint (Figure 3). Ti6Al4V side of the keyhole presents higher temperature than steel side, because of higher absorption coefficient of solid and liquid material. However, the mismatch in thermophysical properties of the materials compensate this difference and final proportion between melted materials is close to 50/50.

The evolution of weld penetration at joint line reflects the progression of development of the keyhole (Figure 4.a). Good correspondence with experimental values is observed for low pulse duration. Above 3 ms, experimental penetration becomes more important. For taking in account this effect, more accurate representation of absorption coefficient on keyhole walls and bottom should be introduced.

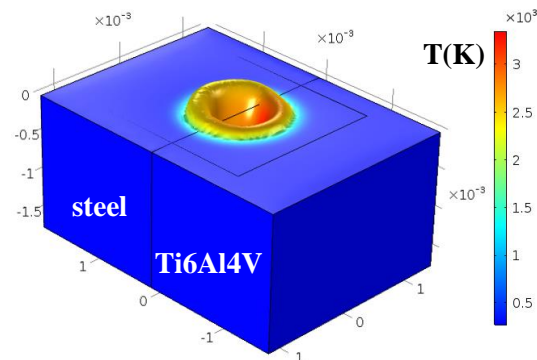


Figure 3. Thermal field of Ti6Al4V/ steel joint after 4 ms impact with laser power of 1.5 kW.

The progress of melting at each side of the joint is represented by evolution of melted zone width with pulse duration (Figure 4.b and c). At present stage, the calculation does not reflect temporary fluctuations of liquid surface created by local impurities, by variation of surface roughness etc., but it reflects well the general tendency in development of melted zone.

It was observed, both numerically and experimentally, that at initial stages of melted zone formation, melting at Ti6Al4V side is more rapid than melting of steel side, but after several ms melting of both sides becomes almost symmetrical.

The comparison between high speed camera images and top view of numerical melted zone

(Figure 5) show that the model allows to approach the form of impact and reflect the evolution of the shape of ejected liquid.

The evolution of keyhole shape at initial stages of melted zone formation (Figure 6) indicates the initiation of liquid depression at Ti6Al4V side and formation of the keyhole preferentially at Ti6Al4V side up to the pulse time of 2 ms. After, the keyhole becomes almost symmetrical to the joint line.

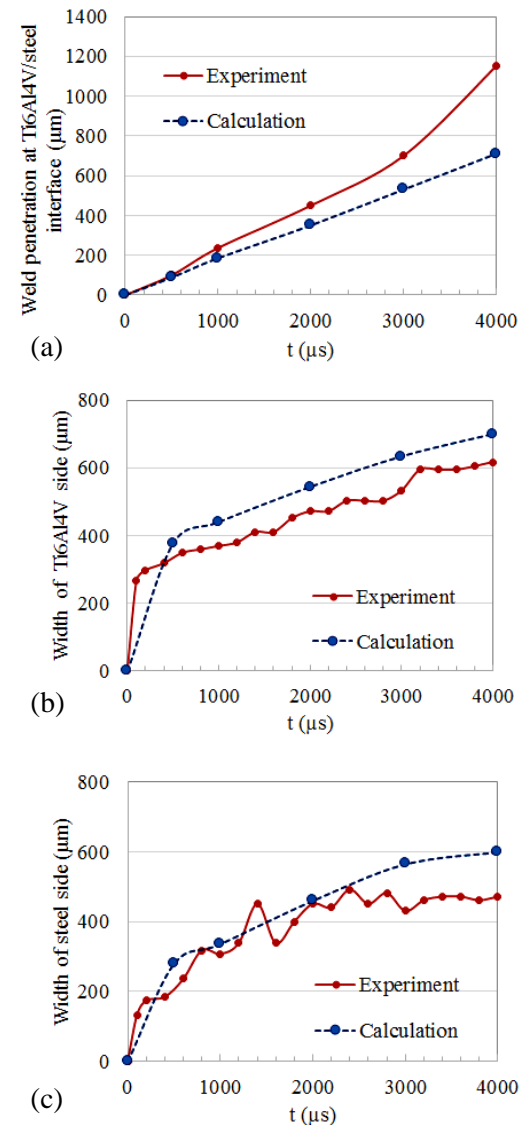


Figure 4. Comparison between experimental and calculated melted zone dimensions 4 ms pulse at Ti6Al4V/ steel interface.

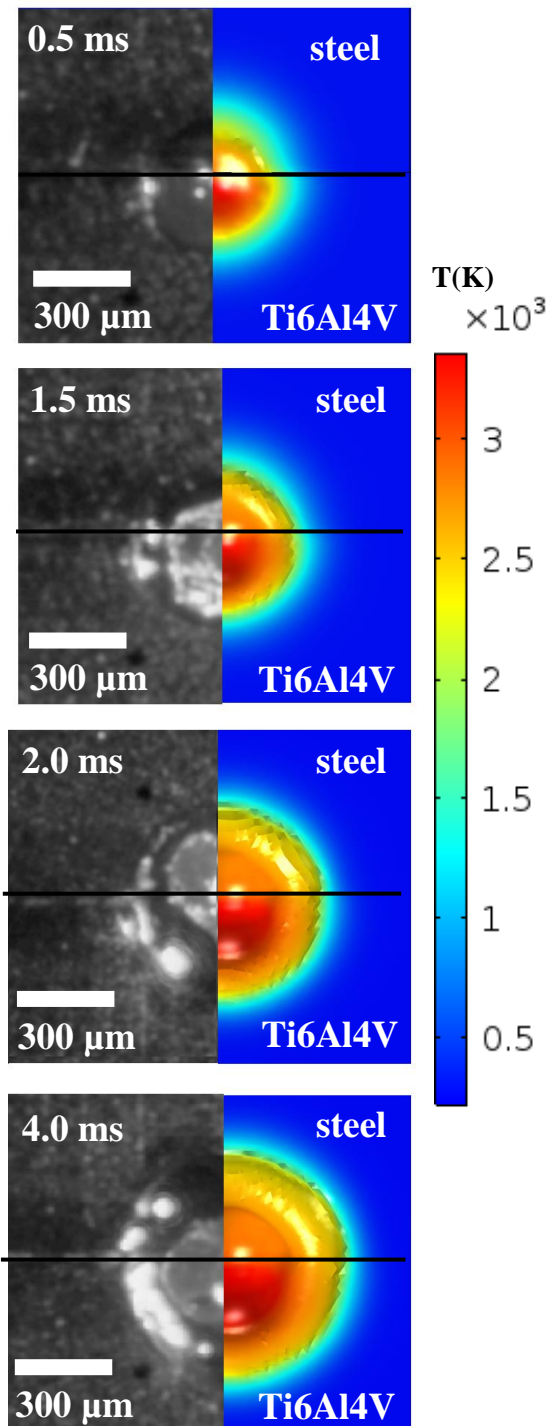


Figure 5. Evolution of impact surface at Ti6Al4V/steel interface: comparison between calculation and high speed camera image (top view).

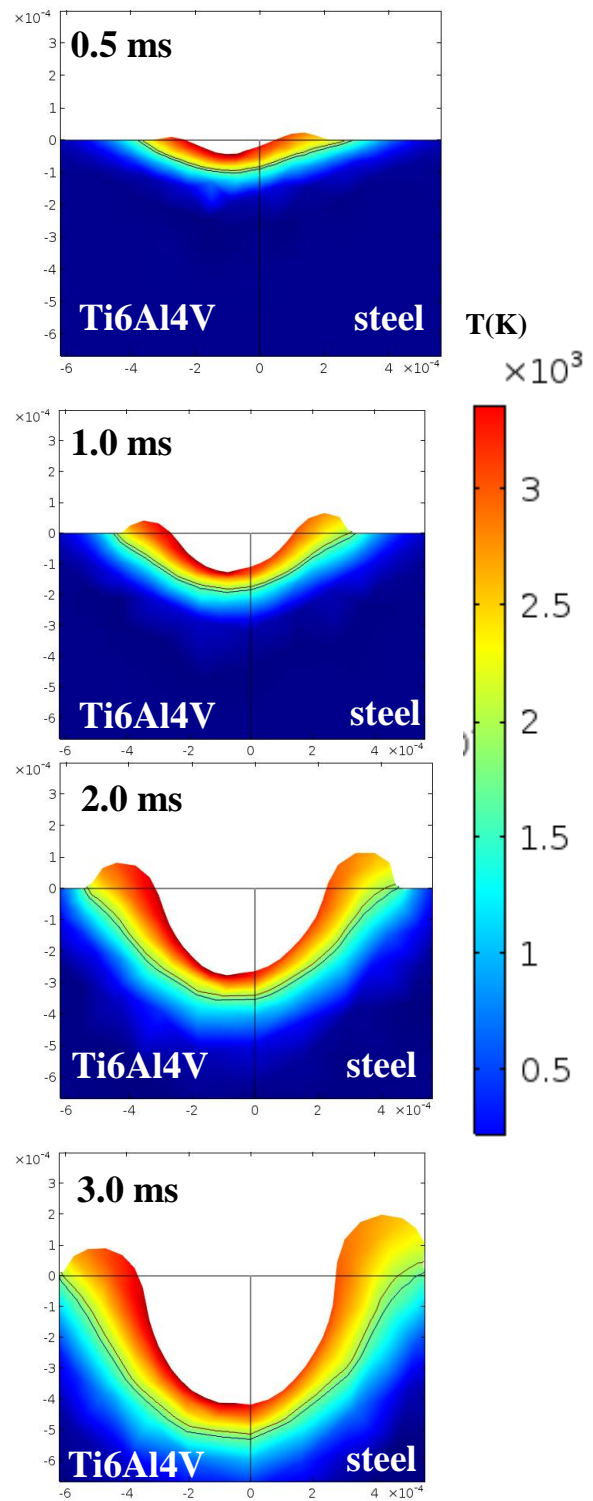
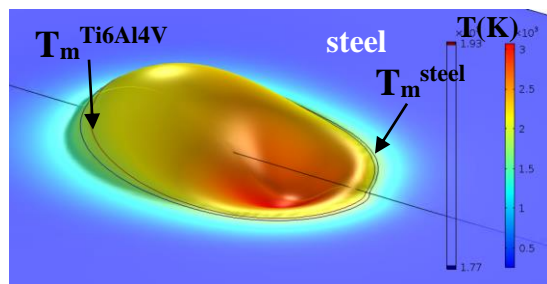


Figure 6. Keyhole development in Ti6Al4V/steel joint (cross view).

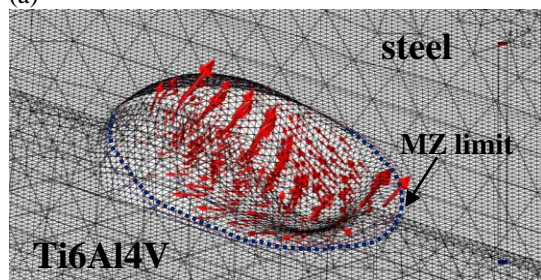
The dimensions of the keyhole are close to the dimensions of focused laser spot (560 μm). This is an important conclusion for proper choice of laser beam position to the joint line.

5.2. Simulation of dissimilar continuous welding between Ti6Al4V and stainless steel

The model was successfully applied to the case of dissimilar Ti6Al4V/steel welding in continuous mode (laser power 1.5 kW, welding speed 8 m/min, spot diameter 560 μm). Taking in account high welding speed and low laser power, after 5 ms of calculation (Figure 7.a) the keyhole only starts to form, and melted material starts to be ejected at the rear. First portion of solidified surface of joint can be observed past fusion isotherm of joined alloys. With higher times of calculation, the present model will be able to provide the surface aspect created by melting and solidification of joined materials.



(a)



(b)

Figure 7. Melted zone view during continuous laser welding of Ti6Al4V/steel joint (laser power 1.5 kW, welding speed 8 m/min, laser spot diameter 560 μm) : thermal field (a) and flow field (b).

After 5 ms of interaction, the width of melted zone at Ti6Al4V and steel sides was found 498 and 473 μm respectively. The same tendency as in pulsed welding is observed: for long

interaction time ($t > 2\text{ms}$), the quantity of melted materials becomes close, in spite of mismatch in fusion temperatures (1928 K for Ti6Al4V and 1773 K for stainless steel). This can be explained by close thermal diffusivities for two welded materials: $7.86 \cdot 10^{-6}$ and $5.58 \cdot 10^{-6}$ m^2/s for Ti6Al4V and steel respectively (at 1500 K). The shape of the capillary is found symmetrical, with maximal width of about 600 μm .

The observation of velocity field (Figure 7.b) gives access to various flows in the melted zone:

- before the keyhole, where melted layer is very thin, metal flows around the capillary;
- past the keyhole, liquid metal rises along keyhole wall and is ejected at the tail part of melted zone;
- on the surface of tail part, liquid metal has a tendency to flow from Ti6Al4V side to stainless steel side, which can be explained by difference in surface tension and viscosity of two liquid metals. This result should be carefully confirmed because no mixing phenomena is not yet introduced to the model.
- finally, Marangoni convection vortex is situated at the volume of liquid past the keyhole.

6. Conclusions

ALE-based multiphysical model of keyhole formation in case of pulsed and continuous welding between dissimilar materials is proposed. First results for pulsed welding were validated for Ti6Al4V/steel couple of materials. The effect of mismatch in physical properties on development of keyhole and of melted zone was quantified. For present couple of materials, the dissymmetry of keyhole to joint line is observed only during first seconds of laser-matter interaction. Same result was found in case of continuous laser welding.

As a perspective of this work, the interdiffusion of species during melting and solidification of the weld will be introduced, which will allow taking in account local variation of thermophysical properties within the melted zone.

The model will also be tested on another dissimilar couples, in order to understand the phenomenology of keyhole formation in case of more important mismatch in physical properties.

9. References

1. I. Tomashchuk, Assemblage hétérogène cuivre-inox et TA6V-inox par les faisceaux de haute énergie: compréhension et modélisation des phénomènes physico-chimiques, *phD thesis, Université de Bourgogne, France* (2010).
2. S.M. Dörfler. Advanced modeling of friction stir welding – improved material model for aluminum alloys and modeling of different materials with different properties by using the level set method, *COMSOL Conference Hannover* (2008).
3. I. Tomashchuk, P. Sallamand, J.M. Jouvard, D. Grevey, The simulation of morphology of dissimilar copper–steel electron beam welds using level set method, *Computational Materials Science*, **48**, 827-836 (2010)
4. A. Métais, S. Matteï, I. Tomashchuk, S. Gaied, Modeling of Transport Phenomena in Laser Welding of Steels, *COMSOL Conference Grenoble* (2015).
5. M.R. Nekouie Esfahani, J. Coupland, S. Marimuthu, Numerical simulation of alloy composition in dissimilar laser welding, *Journal of Materials Processing Technology* **224** 135–142 (2015)
6. V.Bruyere, C. Touvrey, P. Namy, Comparison between Phase Field and ALE methods to model the keyhole digging during spot laser welding, *COMSOL Conference Rotterdam* (2013).
7. C. Bonacina, G. Comini, A. Fassano, M Primicerio, Numerical solutions of phase change problems, *Int. J. Heat Mass Transfer*, **16**, 1825-1832 (1973).
8. S. Morville, Modélisation multiphysique du procédé de fabrication directe par projection laser, *phD thesis, Université de Bretagne-Sud, France* (2012).
9. A.A. Kaidalov, Electron beam welding and annexed technologies (in Russian), Kyiv, Technologia (2004).

10. Acknowledgements

This work was carried out as a part of joint laboratory project LabCom FLAMme between Laboratoire Interdisciplinaire Carnot de Bourgogne, University of Bourgogne-Franche Comté and SME Laser Rhone-Alpes. This project is funded by French National Agency of Research.

Authors would like to thank Dr. Alexandre Mathieu, University of Bourgogne-Franche Comté, France, for his help in rapid camera visualization experiments.